Molecular Engineering of Myoglobin: Influence of Residue 68 on the Rate and the Enantioselectivity of Oxidation Reactions Catalyzed by H64D/V68X Myoglobin†

Hui-Jun Yang,‡ Toshitaka Matsui,§ Shin-ichi Ozaki,|| Shigeru Kato,‡ Takafumi Ueno,⊥ George N. Phillips, Jr.,# Shunichi Fukuzumi,○ and Yoshihito Watanabe*,▽

Department of Structural Molecule Science, The Graduate University for Advanced Studies, Okazaki, Myodaiji 444-8585, Japan, Institute of Multidisciplinary Research for Advanced Materials, Tohoku University, Aoba-ku, Sendai 980-8577, Japan, Department of Biological Chemistry, Yamaguchi University, Yoshida, Yamaguchi 753-8515, Japan, Research Center for Materials Science, Nagoya University, Nagoya 464-8602, Japan, Department of Biochemistry, University of Wisconsin, 433 Babcock Drive, Madison, Wisconsin 53706, Department of Material and Life Science, Graduate School of Engineering, Osaka University, CREST, Japan Science and Technology Corporation, Suita, Osaka 565-0871, Japan, and Department of Chemistry, Graduate School of Science, Nagoya University, Nagoya 464-8602, Japan

Received April 16, 2003; Revised Manuscript Received June 17, 2003

ABSTRACT: In the elucidation of structural requirements of heme vicinity for hydrogen peroxide activation, we found that the replacement of His-64 of myoglobin (Mb) with a negatively charged aspartate residue enhanced peroxidase and peroxygenase activities by 78- and 580-fold, respectively. Since residue 68 is known to influence the ligation of small molecules to the heme iron, we constructed H64D/V68X Mb bearing Ala, Ser, Leu, Ile, and Phe at position 68 to improve the oxidation activity. The Val-68 to Leu mutation of H64D Mb accelerates the reaction with H_2O_2 to form a catalytic species, called compound I, and improves the one-electron oxidation of 2,2′-azinobis(3-ethylbenzothiazoline-6-sulfonic acid) (ABTS) (i.e., peroxidase activity) approximately 2-fold. On the other hand, H64D/V68I Mb oxygenates thioanisole 2.7- and 1600-fold faster than H64D and wild-type Mb, respectively. In terms of the enantioselectivity, H64D/V68A and H64D/V68S Mb were good chiral catalysts for thioanisole oxidation and produced the (*R*)-sulfoxide dominantly with 84% and 88% ee, respectively [Kato, S., et al. (2002) *J. Am. Chem. Soc. 124,* 8506−8507]. On the contrary, the substitution of Val-68 in H64D Mb with an isoleucine residue alters the dominant sulfoxide product from the (*R*)- to the (*S*)-isomer. The crystal structures of H64D/V68A and H64D/V68S Mb elucidated in this study do not clearly indicate residues interacting with thioanisole. However, comparison of the active site structures provides the basis to interpret the changes in oxidation activity: (1) direct steric interactions between residue 68 and substrates (i.e., H_2O_2, ABTS, thioanisole) and (2) the polar interactions between tightly hydrogen-bonded water molecules and substrates.

Heme proteins are generally responsible for the transport of electrons or molecular oxygen, the sensing of molecular oxygen or carbon monoxide, and redox reactions (*1*−*5*). Despite the differences in functions, all of the proteins have heme as a common prosthetic group. Understanding the amino acid residues controlling the intrinsic biological functions of heme is a significant challenge. A common strategy for structure−function studies for a particular enzyme has involved substitution of amino acid residues followed by investigations of the effect of the substitution on the catalytic activity. Instead, we have attempted to convert a nonenzymatic heme protein [i.e., myoglobin (Mb)[1]] into a heme enzyme (i.e., peroxidase). This strategy provides valuable insight into the general structural requirements for the activation of H_2O_2 (*6*, *7*).

We have proved that the distal histidine of sperm whale Mb (i.e., His-64) is a critical residue not only in activating H_2O_2 but also in destabilizing a ferryl porphyrin radical cation, a catalytic species called compound I (Scheme 1) (*8*−*11*). The replacement of His-64 with a hydrophobic amino acid such as Ala and Leu significantly decreases the reactivity with H_2O_2. Although H_2O_2 is not an efficient oxidant for the mutants to produce compound I, *m*-chloroperbenzoic acid (*m*CPBA) can be used as a good substitute. Consequently, compound I has been successfully observed for the distal histidine deletion mutants. On the contrary, compound I of the wild type is not detected with H_2O_2 or *m*CPBA because of its simultaneous decay to compound II (i.e., a ferryl species).

† This work is supported by Grants-in-Aid for Scientific Research 11228208 and 14209019 to Y.W., 13740384 to T.U., and 13780496 to S.O.

* Corresponding author. Tel: (+81) 52-789-3049. Fax: (+81) 52-789-2953. E-mail: yoshi@nucc.cc.nagoya-u.ac.jp.

‡ The Graduate University for Advanced Studies.

§ Tohoku University.

|| Yamaguchi University.

⊥ Research Center for Materials Science, Nagoya University.

University of Wisconsin.

○ Osaka University.

▽ Department of Chemistry, Graduate School of Science, Nagoya University.

[1] Abbreviations: Mb, myoglobin; ABTS, 2,2′-azinobis(3-ethylbenzothiazoline-6-sulfonic acid); *m*CPBA, *m*-chloroperbenzoic acid; HPLC, high-pressure liquid chromatography; EPR, electron paramagnetic resonance; EDTA, ethylenediaminetetraacetic acid; CPO, chloroperoxidase from *Caldariomyces fumagus*.

10.1021/bi034605u CCC: $25.00
Published on Web 08/09/2003

Scheme 1: Peroxidase and Peroxygenase Reaction Cycle

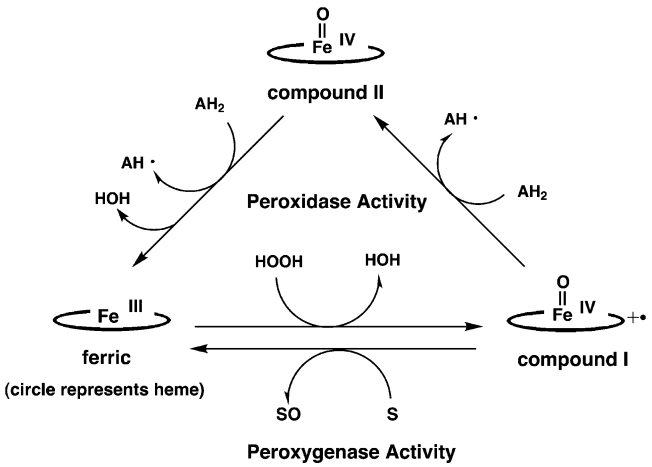

Interestingly, the substitution of His-64 with a negatively charged aspartate residue accelerates the reaction with H_2O_2 and improves peroxidase (i.e., one-electron oxidation) and peroxygenase activity (i.e., two-electron oxidation associated with a ferryl oxygen transfer) (Scheme 1) (*12*). Among the distal histidine deletion mutants, H64D Mb is the best enzyme engineered for the oxidation in the presence of H_2O_2. However, the H64D mutant does not exhibit high enantioselectivity for the sulfoxidation of thioanisole (i.e., 6% ee) (*12*). Thus, we previously performed the mutagenesis of Val-68 in H64D Mb to improve the enantioselectivity because residue 68 as well as residue 64 (i.e., His-64 and Val-68 in wild-type Mb) is known to influence the association and dissociation rate constants for ligand binding (e.g., O_2 and CO) (Figure 1) (*13*, *14*). The replacement of Val-68 of H64D Mb with a smaller alanine residue was found to increase the enantioselectivity of thioanisole oxidation from 6% to 84% ee without losing the catalytic activity significantly (*15*). H64D/V68S Mb also exhibited high enantioselectivity (i.e., 88% ee), but the polar Ser-68 retarded the sulfoxidation rate by approximately half (*15*). Although association and dissociation rate constants of α-methylbenzylamine for H64D/V68A and H64D/V68S Mb were determined to gain insight on high enantioselectivity for the peroxygenation of thioanisole, the active site structures of the mutants were not available (*15*). In addition, the influence of Val-68 on peroxidase activity has not been investigated yet.

As the extension of our previous studies on the Val-68 mutations in H64D Mb (*15*), we report herein further characterization of H64D/V68X Mb bearing Ala, Ser, Leu, Ile, and Phe at position 68: (1) crystal structures of H64D/V68A and H64D/V68S Mb, (2) peroxidase activity of H64D/V68X Mb, (3) peroxygenase activity of H64D/V68L, H64D/V68I, and H64D/V68F Mb, and (4) α-methylbenzylamine binding studies for H64D/V68L, H64D/V68I, and H64D/V68F Mb.

EXPERIMENTAL PROCEDURES

Materials. All chemicals were obtained from Wako or Nacalai Tesque and used without further purification. The buffers used for the reactions were 50 mM sodium phosphate (pH 7.0), 50 mM sodium acetate (pH 5.0), or 20 mM Tris-HCl (pH 9.0).

Preparation of Myoglobin Mutants. The H64D/V68X sperm whale myoglobin mutants (X represents A = Ala, S = Ser, V = Val, I = Ile, L = Leu, or F = Phe) were constructed by cassette mutagenesis. The expression vector of wild-type sperm whale Mb was a gift from Dr. J. S. Olson (Rice University, Houston, TX). The cassette including desired His-64 and Val-68 substitutions and a new silent *Hpa*I restriction site was inserted between the *Bgl*II and *Hpa*I sites. Expression in *Escherichia coli* strain TB-1 and purification of the mutants were performed by following previous reports (*16*, *17*). To ensure that the proteins used in the experiments were all in the ferric form, the sample was oxidized by the addition of a small excess of potassium ferricyanide. An excess oxidant was subsequently removed by gel filtration on a column packed with Sephadex G-25 equilibrated with the reaction buffer. The purified protein was stored at −80 °C until used.

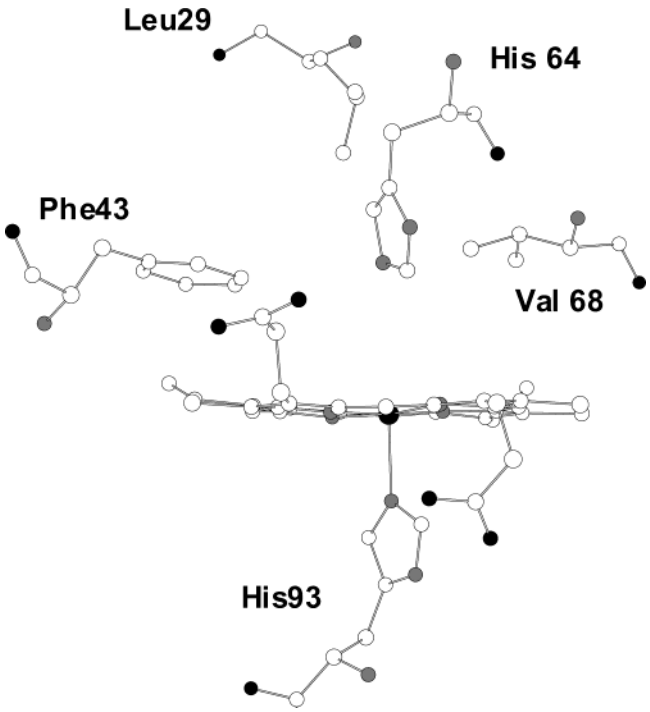

FIGURE 1: Amino acid residues surrounding the heme of sperm whale Mb.

Catalytic Oxidation of ABTS. Activity for one-electron oxidation of ABTS was measured at 20 °C in 50 mM sodium phosphate buffer (pH 7.0) on a Shimadzu UV-2400 spectrophotometer. At least two experiments were performed for each experimental point. The rate of the ABTS cation radical formation was monitored at 730 nm ($\epsilon_{730} = 1.4 \times 10^4$ M^{-1} cm^{-1}) where the absorption of Mb was negligible (*12*). The reaction mixture contained 1 mM ABTS and variable amounts of H_2O_2 (0.2−1.0 mM). The final concentration for H64D/V68X Mb was in the range of 0.05−0.5 μM.

Catalytic Sulfoxidation of Thioanisole. To a solution of either wild-type Mb (5 μM) or a Mb mutant (0.1−0.5 μM) in 0.5 mL of 50 mM sodium phosphate buffer (pH 7.0) were added thioanisole (1 mM) and then H_2O_2 (1 mM) as an oxidant to start the sulfoxidation reaction. After the incubation at 25 °C, the mixture was extracted with dichloromethane for HPLC analysis on a Daicel OD chiral-sensitive column installed on a Shimadzu SPD-10A spectrophotometer equipped with a Shimadzu LC-10AD pump system (*18*). A standard curve prepared with commercial phenyl methyl sulfoxide was used for quantitative analysis. The absolute

stereochemistry was determined on the basis of a retention time. A linear relationship between time versus product formation was observed for at least 5 min for all except for H64D and H64D/V68L Mbs, but the incubations were stopped in 2 min for the determination of rates for all of the mutants. The sulfoxide formed in the control incubation without enzyme was subtracted when necessary.

Reaction with mCPBA or Hydrogen Peroxide. All of the spectral changes were monitored on a Hi-Tech SF-43 stopped-flow apparatus equipped with a MG6000 diode array spectrophotometer. An optical filter (360 nm) was used to avoid possible photoreduction of compound I by the light source (xenon lamp). The reactions with *m*CPBA were carried out at pH 5.0 to observe the complete accumulation of compound I (*10*). The rate constant of thioanisole oxidation by Mb compound I was determined by means of a double-mixing rapid scan technique at 5.0 °C and pH 5.0. The first mixing of ferric Mb with a slight excess of *m*CPBA (1.3−2 mol equiv) resulted in more than 70% accumulation of compound I, which was subsequently mixed with at least a 10-fold excess of thioanisole. The bimolecular rate constants were determined from the observed rates of at least four different concentrations of thioanisole. The reaction for H64D/V68L Mb with H_2O_2 was performed at 20 °C and pH 7.0 because the compound I intermediate was best observed at pH 7.0 when H_2O_2 was an oxidant.

α-*Methylbenzylamine Binding Studies.* All UV−visible measurements were performed at 20 °C on a Shimadzu UV-2400 spectrophotometer. Electronic absorption spectra for H64D/V68X Mbs were recorded in 20 mM Tris-HCl buffer (pH 9.0). Changes of the spin state were monitored on an absorption spectrophotometer by adding aliquots of 1 M (*R*)- or (*S*)-α-methylbenzylamine solution to 3 mL of 4.0 μM protein solution. Spectral changes were monitored until the Soret band did not shift.

Electron paramagnetic resonance (EPR) spectra were recorded on a Bruker E500 X-band CW-EPR spectrometer fitted with an Oxford liquid helium flow-cryostat ESR-910 at a 100 kHz field modulation and 14 K. Highly concentrated ferric H64D/V68X Mb was dialyzed overnight against 20 mM Tris-HCl buffer (pH 9.0) for EPR measurement. To obtain the amine binding complex, the mutants were dialyzed overnight against the same buffer containing 5−20 mM (*R*)- or (*S*)-α-methylbenzylamine, respectively. The color of the amine Mb complex solution changed from brown to dark red during the dialysis.

Kinetic measurements were performed on stopped-flow rapid scan RSP-601 (Unisoku). The initial rate of amine binding was determined at 408 nm using a single wavelength mode. The final concentration was 5.0 μM for Mb and 0−10 mM for (*R*)- or (*S*)-α-methylbenzylamine.

X-ray Crystallography. Crystals were grown in the *P*6 space group using the hanging drop method. Ten microliters of 65 mg/mL HPLC cation-exchange column-purified protein was mixed with a solution of 3.2 M ammonium sulfate, 20 mM Tris-HCl, and 1 mM EDTA (pH 9.0) to give a final concentration of 2.4−2.6 M ammonium sulfate (*11*). The hanging drops were set up at room temperature and incubated at 4.0 °C. The crystal was mounted, and the diffraction data were collected at room temperature. The crystals were mounted in capillaries and the diffraction data were collected at room temperature. Data were collected on a Siemens Hi-Star detector and processed using XDS software (*19*). The H64D/V68S mutant crystals produced a data set that was 89.7% complete to a resolution of 1.95 Å with an *R*-merge of 0.063. The H64D/V68A crystals produced a data set that was 93.8% complete to 1.7 Å resolution with an *R*-merge of 0.088. The structures were solved using the 2MBW wild-type PDB entry (*20*) and refined using CNS (*21*) to final values for *R* and *R*-free of 0.168 and 0.202 for H64D/V68A and 0.160 and 0.190 for H64D/V58S. The structures and the diffraction data have been deposited at the Protein Data Bank as 1LUE (H64D/V68A) and 1O16 (H64D/V68S).

Molecular Modeling. Model building and calculations were performed with InsightII/Discover 3 (Accerlys) in vacuo by using the ESFF force field. (*R*)- and (*S*)-α-methylbenzylamines were constructed with the Builder module of the InsightII package. The distance between iron and nitrogen of the amine was constrained with 2.3 Å. Reconstitution of the amine binding complexes was performed using Biopolymer modules based on the X-ray structures of 1LUE (H64D/V68A Mb) and 1O16 (H64D/V68S Mb).

RESULTS

Crystal Structures of H64D/V68A and H64D/V68S Mb. The H64D/V68A and H64D/V68S double mutations do not affect the secondary and tertiary structure of the protein significantly, but the largest changes are observed in the distal side of the heme. The structure of H64D/V68A Mb reveals that the replacement of Val-68 with a smaller alanine residue creates a space near the *δ-meso*-carbon of heme and that Phe-43, Arg-45, and Asp-64 are relocated by the mutation (Figure 2a). The carboxylate of Asp-64 does not point to the heme iron but toward Arg-45 (Figure 2a). The distance between the Oγ atom of Asp-64 and the guanidinium nitrogen atom of Arg-45 is 4.9 Å, which is longer than the hydrogen-bonding distance. However, the hydrogen-bonding network appears to be attained through a water molecule at 3.0, 3.3, and 2.6 Å from the carboxylate oxygen atom of Asp-64, the guanidinium nitrogen atom of Arg-45, and the oxygen atom of propionate in the heme, respectively (Figure 2b). We have also found that the His-64 → Asp/Val-68 → Ala mutation disrupts the hydrogen bond between Arg-45 and the propionate of heme observed in the wild type. Instead, Asp-64 interacts with the propionate through two water molecules in H64D/V68A Mb (W1 and W2 in Figure 2b). The distance between the Oγ atom of Asp-64 and the ferric heme iron is 7.8 Å in H64D/V68A Mb. The water molecule coordinated to the heme iron is not stabilized by direct hydrogen-bonding interaction with Asp-64 but through water molecules in the distal heme pocket. It should be noted that such distal water molecules are not observed in the wild type (*13*). The structures of H64D/V68A and H64D/V68S Mb are virtually superimposable except for residue 68 and the distal water molecules (W5 in Figure 2b,c). Since Ser-68 bears the hydroxyl group, the coordinated and distal water molecules are more tightly hydrogen-bonded than those in the H64D/V68A mutant (Figure 2c). Although the structure of H64D/V68A Mb could not be compared to that of H64D Mb due to the lack of its structural information, the previously solved V68A Mb structure indicates that Ala-68 in H64D/V68A and V68A Mb is almost superimposable (*14*). Therefore, the relocation of Phe-43 and Arg-45 (Figure 2a)

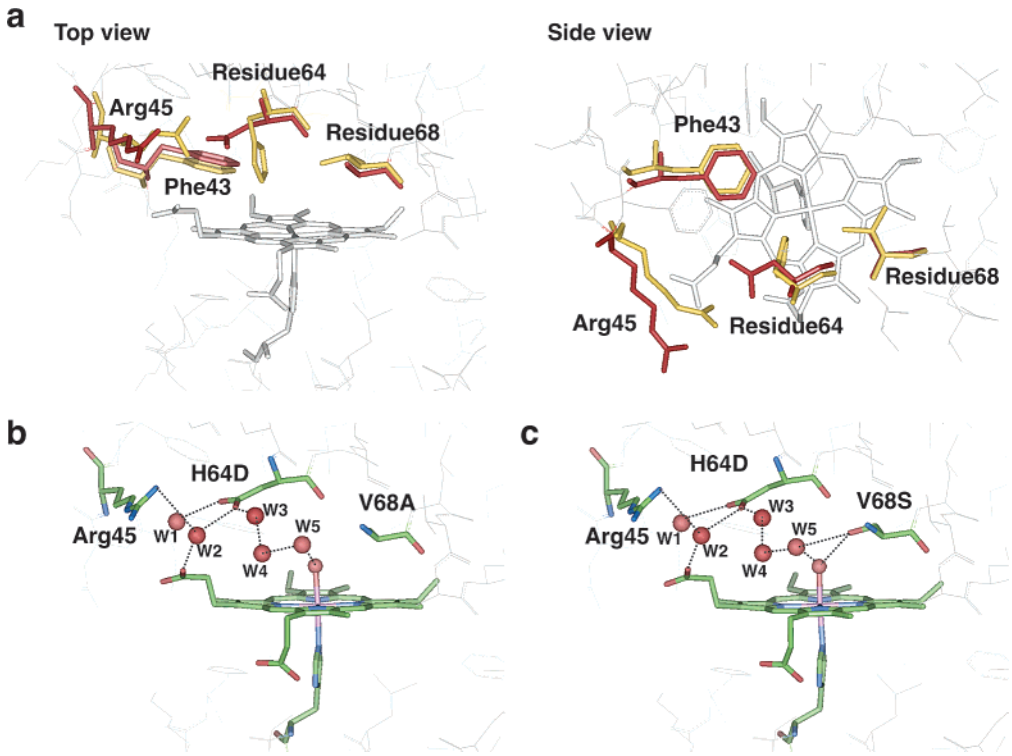

FIGURE 2: (a) Active site residues of H64D/V68A Mb (orange) are superimposed with those of the wild type (yellow). Active site structures of (b) H64D/V68A and (c) H64D/V68S Mb. Red balls represent water molecules.

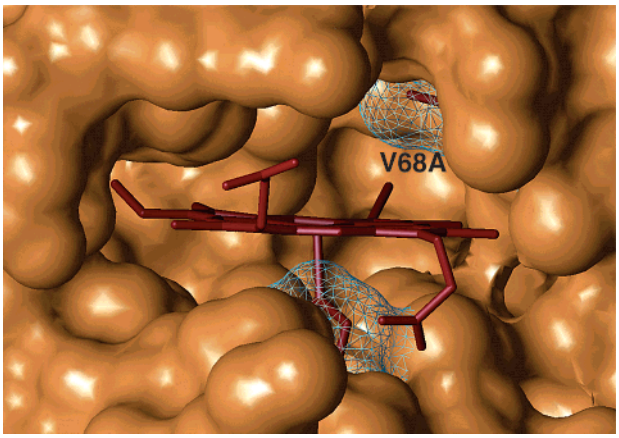

FIGURE 3: Active site structure of H64D/V68A Mb.

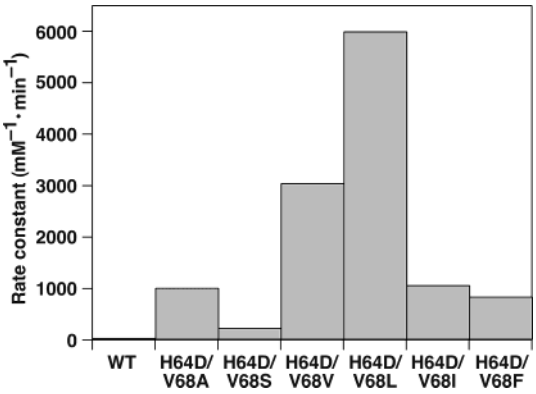

FIGURE 4: Rate constants of ABTS oxidation in the presence of H_2O_2.

appears to be induced by the introduction of an aspartate residue at the position 64.

Since we previously reported that H64D/V68A and H64D/V68S Mb produce the (*R*)-sulfoxide almost exclusively in thioanisole oxidation (*15*), the structural analysis of the mutants provides an active site model for asymmetric oxygen atom transfer reactions (Figure 3). The results suggest that residue 68 is important in the access for the substrate to the heme pocket and that the replacement of Val-68 with various amino acid residues would alter the shape and volume of the heme pocket (Figure 3). Our strategy to design the efficient oxidation catalyst by mutating Val-68 of H64D Mb is supported from the structural viewpoint.

Peroxidase Activity of H64D/V68X Mb. The mutation of Val-68 affects the peroxidase activity, but we do not observe the obvious correlation between the volume of residue 68 and the oxidation rate (Figure 4). Among the H64D/V68X mutants, H64D/V68L Mb exhibits the highest rate for the one-electron oxidation of ABTS. The peroxidase activity for H64D/V68L Mb is approximately 2-fold higher than that of the H64D mutant. H64D/V68I and H64D/V68F Mb, bearing residue 68 larger than Ala, oxidize ABTS at the rate similar to the value for H64D/V68A Mb. However, the activity of the H64D/V68A mutant is approximately 4-fold greater than that for H64D/V68S Mb. The polarity of residue 68 appears to influence the peroxidase activity.

Since the efficiency of the peroxidase cycle is controlled by the reaction of the ferric Mb with H_2O_2, the 150-fold enhancement in peroxidase activity by the H64D/V68L double replacement implies that H64D/V68L Mb reacts with H_2O_2 to form compound I 150-fold faster than the wild type (Figure 4) (*11*, *12*). Furthermore, the lack of an oxidizable distal histidine in the H64D/V68L mutant prevents simultaneous decay of compound I (*10*). Consequently, the ferric state of H64D/V68L Mb is completely converted into compound I with H_2O_2 at a rate of 106 ± 2 s^{-1} (Figure 5). The decrease in the Soret band intensity with the increase

Table 1: Oxidation of Thioanisole by H64D/V68X Mb[a]

	wild type	H64D/V68A	H64D/V68S	H64D	H64D/V68L	H64D/V68I	H64D/V68F
% ee[b]	25	84	88	6.0	3.2	25 (*S*)	46
rate[c]	0.25	120	64	150	260	410	48
vol of residue 68[d]	75	26	33	75	101	102	137

[a] The values of % ee and rate for wild type, H64D/V68A, H64D/V68S, and H64D Mb are taken from our previous study in ref *15*. [b] The absolute stereochemistry of the dominant product is the (*R*)-isomer unless indicated. [c] The unit of rate is turnover/min. [d] The volume is indicated in Å^3. The values are taken from ref *26*.

Table 2: Rate of Thioanisole Oxidation by Compound I[a]

	wild type	H64D/V68A	H64D/V68S	H64D	H64D/V68L	H64D/V68I	H64D/V68F
k	ND	450	ND	220	390	640	220

[a] The unit of *k* is mM^{-1} s^{-1}. ND: compound I of H64D/V68S Mb is not observed due to the rapid decay to compound II.

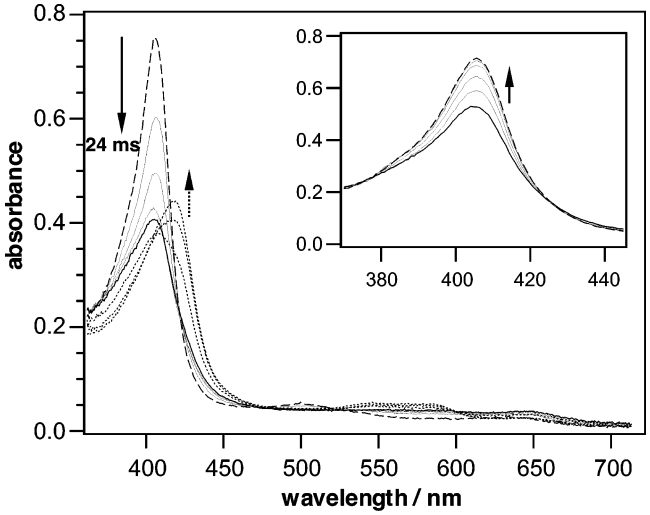

FIGURE 5: Absorption spectral changes of H64D/V68L Mb upon mixing with 1 mM of H_2O_2 at 20 °C in 50 mM sodium phosphate buffer, pH 7.0. The species were recorded before mixing (broken line) and at 6, 12, 20, and 24 ms (solid line) and 0.2, 0.4, and 0.6 s (dotted line) after mixing. (Inset) Reduction of H64D/V68L Mb compound I (thick solid line) in the presence of 100 μM thioanisole. The spectra were recorded before mixing (thick solid line) and 10, 30, 60, 90, and 160 ms (thin solid line and broken line) after mixing.

in the absorption in the visible region is diagnostic of formation of compound I from the ferric state. Upon the addition of thioanisole to the reaction mixture, the intensity of the Soret band is recovered back to the level of the ferric state. To our knowledge, this is the first example of Mb mutant producing almost pure compound I by use of H_2O_2 as an oxidant.

Peroxygenase Activity of H64D/V68X Mb. The peroxygenase activity is examined by using thioanisole as the substrate. The results indicate that residue 68 affects the rate and enantioselectivity of thioanisole oxidation (Table 1). The H64D/V68A and H64D/V68S mutants exhibit equally high enantioselectivity with the (*R*)-sulfoxide as the dominant product.

However, the sulfoxidation rate of H64D/V68S Mb is approximately half of that for H64D/V68A Mb. The polar serine residue at position 68 does not influence the enantioselectivity but decreases the oxidation rate. H64D Mb, bearing valine at residue 68, yields almost a racemic mixture, and the substitution of Val-68 with Ile affords the (*S*)-sulfoxide as the major product with low enantioselectivity. Although the volume of Leu is essentially the same as that of Ile, approximately a 2-fold decrease in the sulfoxidation rate is observed for H64D/V68L Mb compared to that of H64D/V68I Mb. H64D/V68F Mb bearing the most bulky residue at position 68 exhibits the slowest sulfoxidation rate with intermediate enantioselectivity.

To examine the reactivity of compound I of H64D/V68X Mb, we have measured the rate of compound I reduction with thioanisole (Table 2). Typical spectral changes in the reaction of compound I with thioanisole are indicated in Figure 5 (inset). Compound I of H64D/V68X Mb, except for H64D/V68S and wild-type Mb, was generated with *m*CPBA. While the ferric state of H64D/V68L Mb is converted completely into a ferryl porphyrin radical cation with *m*CPBA, compound I of the other mutants is accumulated approximately at the level of 70% on the basis of the Soret intensity. The reaction of H64D/V68S or wild-type Mb with *m*CPBA affords compound II due to the rapid decay of compound I into compound II; therefore, the rate of compound I reduction with thioanisole cannot be determined. The reactivity of compound I for H64D/V68X Mb increases in the order Phe ≤ Val < Leu < Ala < Ile. Although the sulfoxidation rate of H64D/V68A Mb under the steady-state condition is slightly slower than that of H64D Mb (Table 1), compound I reduction with thioanisole for H64D/V68A Mb is faster than that for H64D Mb (Table 2). Since H64D/V68A Mb forms compound I slower than the H64D mutant with H_2O_2 (Figure 4), the results imply that the peroxygenase activity is controlled on the balance between the rate of compound I formation and the efficiency for thioanisole to capture the oxidation equivalents of compound I.

α-Methylbenzylamine Binding for H64D/V68X Mb. The binding of (*S*)- or (*R*)-α-methylbenzylamine to the mutants is a useful probe to examine thioanisole binding orientations because the ligation of nitrogen atom to the ferric heme iron could form a complex similar to an asymmetric transition state expected in thioanisole oxidation (Figure 6). Our previous study indicates that both of the amine isomers associate with H64D/V68A and H64D/V68S Mb at the similar rate, but the dissociation of the (*S*)-isomer is slower than that of the (*R*)-isomer by 27- and 91-fold, respectively (*15*). Therefore, the H64D/V68A and H64D/V68S mutants form stable complexes with the (*S*)-amine. On the other hand, the (*R*)-amine binds to H64D Mb more efficiently than the (*S*)-amine by 7.5-fold but dissociates only by 1.7-fold faster than the (*S*)-amine (*15*). Although the dissociation and

Table 3: Enantioselective Thioanisole Oxidation and Enantiospecific α-Methylbenzylamine Binding[a]

	H64D/V68A	H64D/V68S	H64D	H64D/V68L	H64D/V68I	H64D/V68F
oxidation (% ee)	84 (*R*)[b]	88 (*R*)	6.0 (*R*)	3.2 (*R*)	25 (*S*)	46 (*R*)
amine binding[c]	*S*	*S*	*R*	*R*	*S*	*R* = *S*

[a] The data for H64D/V68A, H64D/V68S, and H64D Mb are taken from our previous study in ref *15*. [b] The dominant product in thioanisole oxidation is indicated. [c] The isomer which exhibits high affinity with the mutant is indicated. H64D/V68F Mb has similar affinity for both of the isomers.

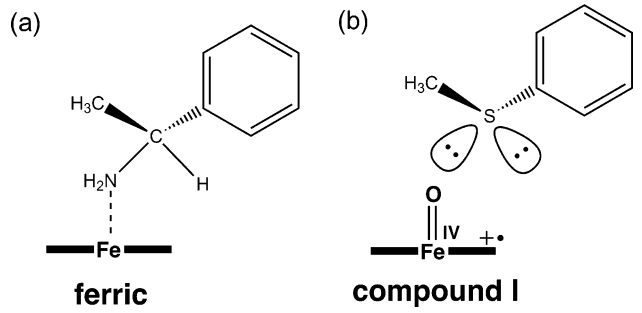

FIGURE 6: Comparison of structures for (a) a α-methylbenzylamine−heme iron complex and (b) an intermediate of thioanisole sulfoxidation.

association rates of α-methylbenzylamine for H64D, H64D/V68A, and H64D/V68S Mb were previously measured (*15*), spectroscopic data of the amine complexes as well as the kinetic parameters of α-methylbenzylamine for the H64D/V68L, H64D/V68I, and H64D/V68F mutants have not been reported. We have examined the remaining work on amine binding for H64D/V68X Mb in this study.

Except for H64D/V68I Mb, the absorption spectrum for the ferric state of the H64D/V68X mutant is similar to that of the wild type with the Soret band at 408 nm, which is typical of hexacoordinated high-spin heme (*22*). On the other hand, the ferric state of H64D/V68I Mb exhibits a blue-shifted Soret maximum at 396 nm, which suggests that the heme iron is in the pentacoordinated high-spin state (*13*). Upon the addition of (*S*)-α-methylbenzylamine to the ferric form of H64D/V68X Mb, the absorption derived from the ferric high-spin heme disappears, and the Soret band shifts to 413 nm with a β-band at 532 nm and an α-band shoulder around 560 nm (Figure 7a). The absorption spectrum is typical for the hexacoordinated ferric low-spin state (*23*). EPR spectral changes also support the conversion of the spin state. The ferric H64D/V68A mutant exhibits rhombically split signals at $g = 6.0$ and 2.0, but the addition of 20 mM (*S*)-α-methylbenzylamine affords new low-spin signals at $g_1 = 3.2$, $g_2 = 2.1$, and $g_3 = 1.4$ (*24*) (Figure 7b). On the other hand, much higher concentration is required to form a complex with (*R*)-α-methylbenzylamine completely.

To determine which isomer has higher affinity with H64D/V68X Mb, the absorption spectral changes were monitored in the presence of a varied amount of either (*S*)- or (*R*)-α-methylbenzylamine (0−30 mM). Unfortunately, we could not measure kinetic parameters for H64D/V68L, H64D/V68I, and H64D/V68F Mb because of the denaturation of proteins in the presence of high amine concentration. However, monitoring the decrease in Soret absorption and appearance of low-spin signals in EPR spectra confirms that the (*S*)-amine binds H64D/V68I Mb and the (*R*)-amine binds H64D/V68L Mb preferentially (Table 3). Although H64D/V68F Mb oxidizes thioanisole to produce the (*R*)-sulfoxide with 46% ee, the mutant has similar affinity for both of the isomers. The dominant configuration produced in the sulfoxidation reaction is not always the same as that in the ligation of α-methylbenzylamine to the heme iron.

DISCUSSION

Influence of Residue 68 on the Rate of Oxidation Activity. The changes in the oxidation activity are interpreted in terms of (1) direct steric interactions between residue 68 and substrates (i.e., H_2O_2, ABTS, thioanisole) and (2) the polar interactions between tightly hydrogen-bonded water molecules and substrates.

Peroxidase activity is known to be a good probe to estimate the efficiency for the ferric Mb mutants to react with H_2O_2 to form compound I (Figure 4). The results indicate that H64D/V68L Mb activates H_2O_2 most efficiently among the H64D/V68X mutants studied here. Interestingly, the Leu-68 → Ile mutation decreases peroxidase activity by 6-fold. The observation suggests that rotation of the substituted side chain about the Cα−Cβ bond is restricted due to branching at the β carbon and prevents the access for H_2O_2 to the heme center. Such a direct steric interaction could explain the decrease in peroxidase activity by the replacement of Leu-68 with Phe. A similar argument was previously used to explain the slower association rate of the oxygen molecule for V68I and V68F Mb with respect to the V68L mutant (*14*). The crystal structure of V68I Mb indicates that the δ-methyl group is located close to the heme iron because branching at the β carbon restricts free rotation of the isoleucine side chain; as a result, the association rate for a ligand to the heme iron decreases. In the case of V68F Mb, the large benzyl side chain of Phe-68 reduces the speed of ligand association.

On the other hand, H64D/V68A Mb exhibits lower peroxidase activity than H64D Mb. The result could not be explained by the direct steric interactions between residue 68 and H_2O_2 because Ala is smaller than Val. On the basis of crystal structures solved in this study, we presume that the distal hydrogen-bonded water molecules might slow the reaction with H_2O_2 because such water molecules have to be replaced by H_2O_2 to react with the heme iron (Figure 2b). The approximately 4-fold decrease in peroxidase activity by the Ala-68 to Ser substitution could be due to the more tightly hydrogen-bonded distal water molecules (Figure 2c). The hydroxyl group of Ser-68 forms additional hydrogen bonds, which are not observed in H64D/V68A Mb, with the distal water molecules.

Peroxygenase activity appears to be controlled by two processes: compound I formation with H_2O_2 and compound I reduction with thioanisole. Since peroxygenase substrates (e.g., thioanisole, styrene) are slower reductants than peroxidase substrates (e.g., ABTS, guaiacol), the efficiency for the peroxygenase substrates to capture the oxidation equivalents of compound I is as important as the rate of compound

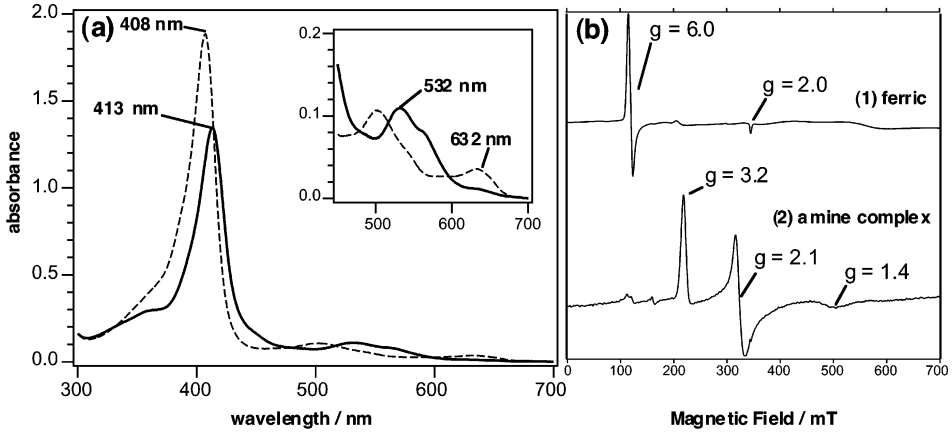

FIGURE 7: (a) Absorption spectrum of the ferric form (dashed line) and the (*S*)-α-methylbenzylamine complex (solid line) of H64D/V68A Mb. (b) EPR spectrum of (1) the ferric form and (2) the (*S*)-α-methylbenzylamine complex of H64D/V68A Mb.

Scheme 2: Possible Functions of Glu-183 of Chloroperoxidase (CPO) in Compound I Formation

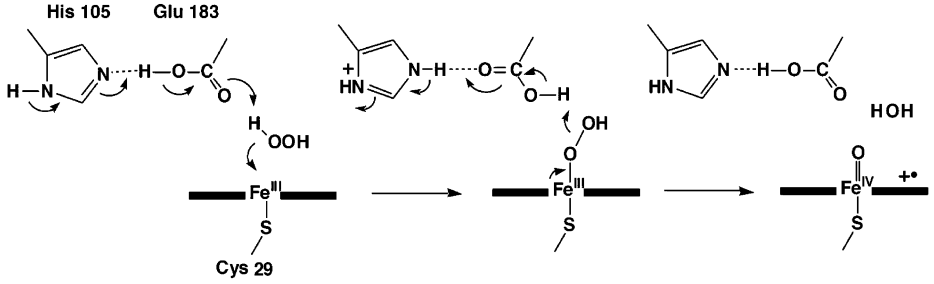

I formation. Although H64D and H64D/V68L Mb react with H_2O_2 to form compound I faster than the others (Figure 4), the rates of compound I reduction with thioanisole are slower than the values for H64D/V68I and H64D/V68A Mb (Table 2). On the contrary, H64D/V68I and H64D/V68A Mb do not form compound I efficiently with H_2O_2 (Figure 4), but thioanisole appears to capture the oxidation equivalents of compound I for the mutants (Table 2). As the results show, H64D/V68A and H64D/V68I Mb exhibit better peroxygenase activity than H64D and H64D/V68L Mb under steady-state condition (Table 1). It seems that peroxygenase activity is regulated on the balance between the rate of compound I formation with H_2O_2 and the efficiency for thioanisole to capture the oxidation equivalents of compound I.

Influence of Residue 68 on the Enantioselectivity in Peroxygenase Activity. The Val-68 → Ala mutation improves the enantioselectivity for thioanisole oxidation from 6.0% to 84% ee with the (*R*)-isomer as the dominant sulfoxide product (Table 1). Since the replacement of Ala-68 with Ser does not alter the value of % ee significantly, the polarity of residue 68 does not seem to influence the enantioselectivity. On the contrary, H64D/V68I Mb affords the (*S*)-methyl phenyl sulfoxide as a dominant product with 25% ee. The branching methyl group at the β carbon of Ile-68 might somehow change the binding mode of thioanisole.

Thioanisole and methyl phenyl sulfoxide were used to study the substrate binding orientation without any success due to the low affinity with the mutants. Thus, we have decided to make a complex with (*R*)- and (*S*)-α-methylbenzylamine to estimate the stability of the transition state for (*R*)- and (*S*)-sulfoxide formation, respectively. Our previous studies indicate that H64D/V68A and H64D/V68S Mb, producing the (*R*)-sulfoxide with high enantioselectivity, exhibit high affinity with (*S*)-α-methylbenzylamine (*15*). Since the association rate constants for the (*S*)- and (*R*)-amine for the mutants are essentially the same, the preference in affinity is controlled by the dissociation rate constants. If we assume that the stability of the amine complex is in parallel with that of the sulfoxidation intermediate, the intermediate to afford the (*S*)-sulfoxide is lower in energy level than the intermediate to the (*R*)-sulfoxide. Consequently, the activation energy for the Fe−O bond cleavage to form the (*R*)-sulfoxide is smaller, and the rate is faster than that for the (*S*)-sulfoxide. Thus, H64D/V68A and H64D/V68S Mb produce the (*R*)-sulfoxide with high enantioselectivity.

Since we found in this study that H64D/V68I Mb oxidized thioanisole to produce the (*S*)-sulfoxide as a dominant product with 25% ee, we were especially interested in kinetic parameters of α-methylbenzylamine for the H64D/V68I mutant. Although absorption and EPR spectral changes confirm the ligation of the nitrogen atom to the heme iron, the exact association and dissociation rates could not be determined for H64D/V68I as well as H64D/V68L and H64D/V68F Mb due to the instability of the mutants with high amine concentration.

Crystal Structures of H64D/V68A and H64D/V68S Mb. Crystal structures of H64D/V68A and H64D/V66S Mb provide us with some important structural information to understand the roles of distal residues in oxidation reactions (Figure 2). The distal histidine of Mb (i.e., His-64 in Mb) is replaced with Asp to mimic chloroperoxidase (CPO), in which Glu-183 and His-105 cooperatively function as catalytically important amino acids in compound I formation (Scheme 2) (*12*, *25*). In H64D/V68A Mb, Asp-64 is pointed toward Arg-45 by hydrogen-bonding interactions via a water molecule, and the Oγ atom of Asp-64 is separated from the heme iron by 7.7 Å (Figure 2b). The value is 2.5 Å longer than the distance between the carboxylate oxygen atom of

Glu-183 and the heme iron in CPO (*25*). From a structural viewpoint, Asp-64 in H64D/V68A Mb does not seem to be involved directly in compound I formation as proposed to Glu-183 in CPO (Scheme 2). The conclusion is consistent with our previous studies on H64D Mb utilizing hydrogen cyanide and cumene hydroperoxide as probes to examine the roles of Asp-64 (*12*).

Although Asp-64 of H64D/V68A Mb is not expected to function as Glu-183 of CPO in the activation of H_2O_2, the negatively charged aspartate residue allows the distal heme pocket of the mutant to accommodate some distal water molecules, which are not found in the wild type. We speculate that such a polar distal heme pocket of the mutant increases the affinity with H_2O_2 and improves the oxidation activity compared to the wild type. However, water molecules in the heme pocket have to be replaced with substrates (e.g., H_2O_2, ABTS, and thioanisole) during the reaction, and strongly hydrogen-bonded water molecules could retard the process. The lower oxidation activity of H64D/V68S than H64D/V68A Mb might be explained by additional hydrogen-bonding interactions between Ser-68 and the distal water molecules revealed in the crystal structure (Figure 2b,c). The variance in reactivity with H_2O_2 for the H64D/V68X mutants may be explained by the difference in arrangement of distal water molecules.

H64D/V68A and H64D/V68S Mb share some common structural features (Figure 2): Asp-64 is pointed at Arg-45 by hydrogen-bonding interactions, and the replacement of Val-68 with smaller Ala or Ser creates a open space to have some hydrogen-bonded water molecules in the distal side. Thus, both of the mutants appear to accommodate bulky substrates if the distal water molecules are replaced. The structures support the relatively fast association rates of α-methylbenzylamine (*15*) and the access for thioanisole to the ferryl oxygen atom (Tables 1 and 2). The residues interacting with the aromatic group of α-methylbenzylamine or thioanisole are not clear at the moment. However, the preliminary molecular calculation starting from the crystal structure of H64D/V68A or H64D/V68S Mb suggests that the complex with (*S*)-α-methylbenzylamine is more stable than the counterpart by 3.4 and 2.0 kcal/mol, respectively. Structural analyses of the other H64D/V68X mutants as well as (*S*)- or (*R*)-α-methylbenzylamine complexes are awaited for further discussion.

In summary, we have successfully improved the peroxidase activity by replacing Val-68 with Leu in H64D Mb. The Val-68 → Leu or Ile mutation of H64D Mb enhances the peroxygenase activity. The improvement in enantioselectivity for the peroxygenase reaction is attained by Val-68 → Ala or Ser. Our results clearly indicate that residue 68 affects both the rate and enantioselectivity of the oxidation reactions. The changes in oxidation activity of H64D/V68X Mb are interpreted in terms of direct steric interactions of residue 68 and substrates (i.e., H_2O_2, ABTS, thioanisole) and polar interactions of the distal water molecule with substrates. The kinetic parameters of α-methylbenzylamine ligation and crystal structures of the H64D/V68A and H64D/V68S Mb support our interpretation.

REFERENCES

1. Antonini, E., and Brunori, M. (1971) *Hemoglobin and Myoglobin in Their Reactions with Ligands*, North-Holland Publishing Co., Amsterdam.
2. Dunford, H. B. (1999) *Heme Peroxidases*, Wiley-VCH, New York.
3. Moore, G. R., and Pettigrew, G. W. (1990) *Cytochromes C*, Springer-Verlag, New York.
4. Ortiz de Montellano, P. R. (1995) *Cytochrome P450*, 2nd ed., Plenum Press, New York.
5. Rodgers, K. R. (1999) *Curr. Opin. Chem. Biol. 3*, 158−167.
6. Ozaki, S., Matsui, T., Roach, M. P., and Watanabe, Y. (2000) *Coord. Chem. Rev. 198*, 39−59.
7. Ozaki, S., Roach, M. P., Matsui, T., and Watanabe, Y. (2001) *Acc. Chem. Res. 34*, 818−825.
8. Ozaki, S., Matsui, T., and Watanabe, Y. (1996) *J. Am. Chem. Soc. 118*, 9784−9785.
9. Ozaki, S., Matsui, T., and Watanabe, Y. (1997) *J. Am. Chem. Soc. 119*, 6666−6667.
10. Matsui, T., Ozaki, S., and Watanabe, Y. (1997) *J. Biol. Chem. 272*, 32735−32738.
11. Matsui, T., Ozaki, S., Liong, E., Phillips, G. N., and Watanabe, Y. (1999) *J. Biol. Chem. 274*, 2838−2844.
12. Matsui, T., Ozaki, S., and Watanabe, Y. (1999) *J. Am. Chem. Soc. 121*, 9952−9957.
13. Quillin, M. L., Arduini, R. M., Olson, J. S., and Phillips, G. N. J. (1993) *J. Mol. Biol. 234*, 140−155.
14. Quillin, M. L., Li, T., Olson, J. S., Phillips, G. N. J., Dou, Y., Ikeda-Saito, M., Regan, R., Carlson, M., Gibson, Q. H., Li, H., and Elber, R. (1995) *J. Mol. Biol. 245*, 416−436.
15. Kato, S., Yang, H.-J., Ueno, T., Ozaki, S., Phillips, G. N., Jr., Fukuzumi, S., and Watanabe, Y. (2002) *J. Am. Chem. Soc. 124*, 8506−8507.
16. Springer, B. A., and Sligar, S. G. (1987) *Proc. Natl. Acad. Sci. U.S.A. 84*, 8961−8905.
17. Wilks, A., and Ortiz de Montellano, P. R. (1992) *J. Biol. Chem. 267*, 8827−8833.
18. Ozaki, S., and Ortiz de Montellano, P. R. (1995) *J. Am. Chem. Soc. 117*, 7056−7064.
19. Kabsch, W. (1988) *J. Appl. Crystallogr. 21*, 67−81.
20. Brucker, E. A., Olson, J. S., Phillips, G. N., Jr., Dou, Y., and Ikeda-Saito, M. (1996) *J. Biol. Chem. 271*, 25419−25422.
21. Brunger, A. T., Adams, P. D., Clore, G. M., Delano, W. L., Gros, P., Grosse-Kunstleve, R. W., Jiang, J. S., Kuszewski, J., Nilges, N., Pannu, N. S., Rice, L., M,, Simonson, T., and Warren, G. L., 1998. (1988) *Acta Crystallogr. D54*, 905−921.
22. Takano, T. (1977) *J. Mol. Biol. 110*, 537−568.
23. Iizuka, T., and Yonetani, T. (1970) *Adv. Biophys. 1*, 157−182.
24. Adachi, S., Nagano, S., Ishimori, K., Watanabe, Y., Morishima, I., Egawa, T., Kitagawa, T., and Makino, R. (1993) *Biochemistry 32*, 241−252.
25. Sundaramoorthy, M., Terner, J., and Poulos, T. L. (1995) *Structure 3*, 1367−1377.
26. Creighton, T. E., Ed. (1983) *Proteins*, W. H. Freeman, New York.

BI034605U